Detecting gas leakage using high frequency signals generated by air gun arrays

by

M. Landrø[1], F. Hansteen[2] and L. Amundsen[1]

[1]*NTNU, 7491 TRONDHEIM, NORWAY*
[2]*STATOIL, NORWAY*

ABSTRACT

Recent field experiments have demonstrated that marine air gun arrays create acoustic energy above 1 kHz. In this work, we suggest to use the high-frequency signal as a source to look for gas leakage at for instance a producing hydrocarbon field, or a CO_2 storage site where the field is covered by permanent acoustic sensors at the seabed, often referred to as a PRM (Permanent Reservoir Monitoring) field. The only needed modification is that the temporal sampling interval for the receivers is decreased to 0.1 ms (in contrast to the normal sampling interval of 1 or 2 ms), to ensure that the system is capable of recording signals up to 5 kHz. We suggest using numerous fixed receivers at the seabed to detect a gas chimney by simple high-pass filtering and subsequent transmission type analysis of the recorded signals. We think this method might serve as an elegant, precise, and very cost-effective way to detect gas leakage into the water layer.

INTRODUCTION AND BACKGROUND

Natural-gas seepage is the steady or episodic, slow or rapid, visible or invisible flow of gaseous hydrocarbons from subsurface sources to Earth's surface (Etiope, 2015, Hovland and Judd, 1988). Gas seepage is well known to take place in relation to

conventional petroleum in sedimentary basins as well as gas hydrate accumulations. In addition, gas may leak from man-made activities like hydrocarbon drilling and CO_2 injection.

In marine settings, a number of techniques for detecting and measuring gas seepage have been developed. The book of Etiope (2015) provides a representative overview of current methodologies. Recent advances include sonar systems which are capable of providing images of micro-seeps large enough to produce bubbles in the water column.

After the successful time-lapse monitoring of the Gullfaks field (Landrø et al., 1999) in the North Sea, there was a strong focus on how to repeat two (or more) surveys as accurately as possible (Landrø, 1999; Calvert, 2005), and in 2003 BP introduced the Life of Field Seismics (LoFS) (Barkved, 2004) at the Valhall field. By installing the receiver array at the seabed (actually trenched approximately half a meter into the seabed) the accuracy of time-lapse seismic data was increased significantly. In addition to this, the monitor surveys are cheap since they only involve a single shooting vessel covering the whole field within some weeks. At present, four hydrocarbon fields offshore Norway use this type of permanent reservoir monitoring (PRM) system: Valhall, Ekofisk, Snorre and Grane.

In this article, we suggest an alternative method for gas-leakage detection or detection of other un-intended leaks or changes close to the seabed that exploits the fact that marine air gun arrays generate high-frequency signals that are detectable over a range of several kilometers. Typically, repeated seismic surveys are acquired at PRM fields twice a year by using a dedicated supply vessel equipped with a source array. We

suggest to exploit these repeated acquisitions to monitor and eventually detect gas leakage directly into the water column by using the high-frequency signals generated by the source array.

Landrø et al. (2011) discuss the frequency properties and possible causes for the high-frequency signals. They suggest that the mechanism of ghost cavitation can cause a significant amount of high-frequency signals emitted from an air gun array. The more guns and the closer they are, the more the ghost cavitation effect will contribute to the high-frequency signals. A dedicated experiment was performed in 2011 where this hypothesis was further tested by for instance increasing the distance between two subarrays in a seismic array (Landrø et al., 2016). They found that the strength of the high-frequency signals was reduced by increasing the distance between subarrays from 6.5 to 8 m.

SIMPLE MODELING OF RESPONSE OF A GAS CHIMNEY

A 1 kHz signal that propagates in water has a typical wavelength of 1.5 m, and at 5 kHz a corresponding wavelength of 0.3 m. This means that objects of the order of meters can be detected, given that there are sufficient changes in water velocity caused by the gas chimney. We assume that we can use ray tracing to model the high-frequency signals generated by the air gun array. The simple model sketched in Figure 1 illustrates the method. From the geometry shown in this figure we find that the distance traveled within the gas chimney, *c*, is given as

$$c = 2\sqrt{a^2 - \frac{d^2 x^2}{x^2 + y^2}}\,, \qquad (1)$$

where a is the radius of the chimney, *d* is the distance from the source to the center of the chimney, *x* is the offset along a receiver line that is perpendicular to the line defined

by the shot and the chimney center, and *y* is the distance from the shot to the receiver line. For a field case, there will be many more receiver locations available than along such a single line, so this example is used for demonstration purposes only. If we assume that the spatial sampling is limited along the receiver line, we observe that this can be compensated by increasing the distance from the chimney to the receiver line. When *c* is known, it is straightforward to derive the traveltime t_0 for the case without a chimney and t_1 for the case including the gas chimney:

$$t_0 = \frac{1}{v_0}\sqrt{x^2 + y^2}\ , \tag{2}$$

$$t_1 = t_0 + c\left(\frac{1}{v_1} - \frac{1}{v_0}\right), \tag{3}$$

where v_0 is the P-wave velocity in the water layer without any gas leakage and v_1 is the P-wave velocity within the gas chimney. Figure 2 (top) shows examples of modeled traveltime curves with and without gas leakage, for chimney radii of 5 and 1 m, respectively. In this example, we have assumed that the water velocity decreases from 1500 m/s outside the gas chimney to 500 m/s inside the gas leakage area. Using Wood's formula (Wood, 1955) for a mixture of water and air, and assuming for instance 0.05 % air, we get a velocity of 500 m/s for this water-air mixture. In the current example, we have used *d* = 500 m and *y* = 1000 m. We observe detectable traveltime changes in both cases: Of the order of 12 ms for the 5 m case and less, but still observable (2 ms) for the 1 m case.

If the receiver line is not perpendicular to the gas chimney, but rotated by an angle φ, the above equations are slightly altered, since the length to the receiver line is changed by the correction distance z_c (Figure 1):

$$z_c = x\frac{\sin(\varphi)}{\cos(\theta-\varphi)}\text{, where } \theta = \arctan\left(\frac{x}{y}\right). \quad (4)$$

The corresponding shortest distance to the rotated receiver line is now

$$y' = y\cos\varphi \quad (5)$$

and the new x-position is given as

$$x' = y'\tan(\varphi-\theta) = y\sin\varphi - x\frac{\cos\varphi}{\cos(\theta-\varphi)}. \quad (6)$$

A third and slightly more computationally heavy method is to use cross-correlation to estimate the deviation from the estimated traveltime (assuming a constant water velocity) for every shot-receiver pair in the survey. If we have *N* sources and *M* receivers it means *NxM* crosscorrelations. To illustrate this technique for a realistic synthetic case, we have computed this time difference ($dt=t_1-t_0$) using the acquisition configuration as for the Snorre and Grane PRM (Thompson et al., 2015). This means that the shot grid is 50 m x 50 m and the receiver grid is 50 m x 300 m (300 m between receiver cables). Assuming an area of 10 km x 10 km, this yields 201x201 shots (*N* = 40401) and 33 receiver cables with 201 receivers in each cable, that is *M* = 6633. Assuming a circular gas leak with a radius of 1 m, we estimate the traveltime shift for all rays that intersect the gas-leak area. We keep only those rays that have a relative time shift larger than 0.25%. In a subsequent analysis we calculate all possible intersections between the detected rays. Figure 2 (bottom) shows the estimated intersections as a scatter plot. We notice that most of the intersections are within the gas anomaly, which is a circle with a radius of 1 m in this case. We clearly see that the large amount of data will help us to estimate the anomaly at the correct position. This enormous multiplicity in the data may also be exploited to find correct source positions. Assuming a constant background water velocity, and estimating precise traveltimes for each source-receiver pair, we suggest to use crosscorrelations again to adjust the source positions to their correct positions, prior to the detection

algorithm described above. The proposed method clearly depends on that the high-frequency signal is above the background noise level, and that the correlation method enables traveltime shift estimations with an accuracy of approximately 1 ms. This issue will be addressed in the following section.

RANGE OF THE HIGH-FREQUENCY SIGNAL

In the examples shown above we have assumed that the high-frequency signal has a practical range of several hundred meters and up to kilometers. This is required if the method should be used for fields that might extend over several square kilometers. To investigate the practical range and signal-to-noise ratio, we use the same field data as described in Landrø et al. (2013), in the section denoted “The field experiment”. In this experiment, a hydrophone located at the sea bottom was used to record far-field signatures from an air gun source that passed as close as possible over the hydrophone. The water depth is approximately 55 m, meaning that the near-offset trace has a source-receiver distance of slightly more than 55 m. The sampling rate is 0.008 ms, corresponding to a maximum frequency of 62.5 kHz. In the following, we will compare the near-offset trace with a far-offset trace corresponding to an offset value of 225 m from the hydrophone. Figure 3a shows the unfiltered near- and far-offset traces from this experiment. In Figure 3b we have applied a 1-5 kHz bandpass filter to the same traces. Then we take the absolute value of each sample, and finally a standard smoothing operator with a window length of 0.8 ms is applied. We notice that most of this high-frequency signal occurs at the same time as the main peak signal (shown in Figure 3a). The strength of the bandpass-filtered signal (1-5 kHz) is approximately 40 times weaker than the unfiltered version. When we normalize the data (Figure 3c), we observe that the high-frequency data is repeatable from the on-set of the primary peak at 78 ms until

approximately 85 ms. After 85 ms we observe larger deviations between the near- and far-offset high-frequency signals. We interpret this increasing difference trend to be caused by the fact that the ghost reflection is very different at near and far offsets. When we apply a 5-10 kHz bandpass filter (Figure 3d), we observe that the high-frequency signal occurs at a much later time: around 94.5 ms for the near-offset trace and 97.5 ms for the far-offset trace. In this case, we attribute the major part of the signal to be caused by the ghost cavitation effect (Landrø et al., 2011, 2013 and 2016). The time shift of 3 ms between the near- and far-offset trace indicates that there is a shift between the onset of the source signature for the near and far offset and the maximum peak amplitude. It might also suggest that the ghost cavity cloud is elongated, as shown in Figure 7 in Landrø et al. (2016). To investigate this time shift further needs more investigation and accurate modeling of both the air gun array and the ghost cavitation process.

When producing Figure 3d we found that the amplitude ratio between the ghost-cavitation signals for near and far offsets is approximately 4.5. The estimated ratio between the raypaths for the near and far offset trace is 4.3. This indicates that the amplitude difference between the near- and far-offset trace is mainly attributed to geometrical spreading. This is expected, since we know that the intrinsic attenuation in water is very low for P-waves, even for frequencies up to 10 kHz. A detailed comparison of the far-offset signal at 225 m and the background noise level gives a signal-to-noise (S/N) ratio of approximately 220. If we assume that a S/N-ratio of 10 is sufficient, this means that a practical range for the 5-10 kHz signal created by a conventional air gun array is approximately 2.3 km, and if we assume S/N-ratio equal to 2 the range is 11.5 km.

CROSSCORRELATION TIME LAGS

The easiest way to estimate traveltime lags between several seismic traces is to cross-correlate them. Figure 4 shows the estimated time lag between the unfiltered near- and far-offset traces (the same traces as shown in Figure 3a). Note that prior to the cross-correlation we have aligned the two traces so that the on-set is the same for both. This means that the maximum peak might occur at a slightly different time for the two traces, since the length of the array causes less spread in traveltimes at zero offset compared to a finite offset. This is probably the main cause for the non-zero time lag observed in Figure 4 for the unfiltered data. According to the crosscorrelation analysis, there is a lag of -1.4 ms between the two traces. For the purpose of this paper, the cause for this time lag is not important, the important issue is that we can estimate time lags for unfiltered data, and compare those to the high-pass filtered data. This crosscorrelation exercise is shown for 1-5 kHz filter (dashed line) and for 5-10 kHz filter (dotted line). For the filtered cases, we have used the same traces as shown in Figure 3 as input to the crosscorrelation (after absolute value and smoothing). We observe a time shift between unfiltered and filtered data of 3.5 and 4.0 ms for the 1-5 and 5-10 kHz filters, respectively. These differences correspond to approximately 5-6 m shift between the source “center of mass” position for the low-frequency signal and the high-frequency signal. The major cause for this shift is most likely due to the head wave that occurs prior to the direct arrival for the far-offset trace. Since the head-wave amplitude is proportional to one over frequency (Aki and Richards, equation 6.26, 2009), the low-frequency crosscorrelation signal will include more of the headwave signal compared to the high-pass filtered versions, which results in longer cross-correlation time lags, as observed in Figure 4. This time shift might also be caused by the elongated shape of the ghost cavitation cloud. The length of the air gun array used in the test is 15 m. However, the purpose of this paper is not to explain the measured time shift, but to

demonstrate that a simple crosscorrelation technique can be used to estimate traveltime curves like those shown in Figure 2, and hence detect the gas anomaly. For the case of a gas leak situation, the unfiltered low-frequency signal will not be delayed by the gas leak, in contrast to the high-frequency signal that will be somewhat delayed. Hence, this difference between low- and high-frequency data might be exploited to detect gas leak.

DISCUSSION

For offshore PRM systems the receiver cables are normally trenched into the seabed, typically at a depth of the order of 1 m. This will introduce attenuation of the high-frequency signal. A simple estimation of how strong this absorption is for a 5 kHz signal can be obtained by using a simple Q-model:

$$A_2 = A_1 e^{-\pi f T / Q} \quad . \qquad (7)$$

Here A_1 is the signal at the seabed and A_2 is the signal measured at the trenched cable for instance 1 m deeper. Assuming a traveltime T for this one meter distance equal to 0.8 ms yields $A_2/A_1 = 0.5$, if $f = 5$ kHz and $Q = 20$. We have chosen a particularly low Q-value in this example for illustration purposes. Most offshore sediments have average Q-values above this one. However, for particular loose seabed conditions, such low values cannot be excluded. This means that the trenching of the cable should not represent a major problem, although we must expect some attenuation, especially for frequencies above 5 kHz.

So far, we have assumed that the gas chimney extends from the seabed to the sea surface. If the chimney has a given height h, which is less than the water depth, this will introduce a constraint on how far it is possible to see the chimney on a receiver line situated behind it. Simple raypath calculation may be used to address this issue further.

The areal extent of the source array and the actual physical mechanism for creating the high-frequency signal is another issue that we have not addressed in this letter. In the same way as your shadow becomes more diffuse and larger if you move towards the light source, we get similar effects if we assume that the source is not a point source but extends over a finite area. Again, simple modeling exercises can be done to investigate how this effect will impact the analysis for a given source array configuration.

The extra cost related to the proposed method is that we need to increase the sampling rate by a factor of 10 or more, depending upon the accuracy requested. For 2 ms sampling, the Nyquist frequency is 250 Hz, yielding a minimum wavelength of 6 m. This means that there should be a potential for detecting reasonable sized gas chimneys without decreasing the sampling rate. However, we think that the possibilities for detecting minor gas leaks increases significantly if the sampling rate is reduced so that we can exploit the high-frequency part of the signal generated by an air gun array.

We think that the strength of this method is related to the fact that you can do this at the same time as regular seismic data is acquired, and the fact that you have so many receivers and shot positions. This huge multiplicity in source-receiver positions will increase the chance of detecting a minor gas leakage into the sea water.

From Figure 3c we observe that the width of the first high-frequency peak is approximately 2 ms while the width of the low-frequency peak (Figure 3a) is close to 4-5 ms). This means that there is a potential for more accurate mapping of changes in the seabed topography as well as near-surface changes beneath the sea bed by exploiting the 1-5 kHz bandwidth for time-lapse seismic analysis.

An alternative method to using the ghost cavitation for leakage detection is to use for instance the echo sounder or acoustic positioning equipment on board the seismic vessel for this purpose. Figure 5 shows a comparison between the echosounder signal and the signal generated by a single 300 cubic inch conventional air gun. The distance from the echosounder to the sea bed hydrophone is approximately 110 m, and the corresponding distance from the air gun to the hydrophone is approximately 60 m. The dominant frequency for the echo sounder in this example is 20 kHz, and it is clearly visible for the 18-22 kHz band-pass filtered data. However, for frequencies between 2 and 10 kHz (red curve) the signal from the echosounder is weak compared to the high-frequency signal generated by a the single air gun. Figure 5 also shows that the high-frequency signal generated by a single air gun occurs some milliseconds prior to the main peak. Coste et al. (2014) showed that the high-frequency signal generated by a single air gun can be reduced by approximately 10 dB for the frequency range between 0.5 to 3 kHz by implementing a new air gun design. The environmental aspects related to the high-frequency signal generated by air gun arrays have been discussed by several authors, see for example Coste et al. (2014) and Landrø et al. (2016).

In this letter, we have assumed a constant water velocity. Osdal and Landrø (2011, Figure 4) shows that typical variations in the water velocity at the Norne Field (offshore Norway) varies between 1485 and 1505 m/s (or 1.3 %). The dominat velocity changes in their example from the Norne field occurs between 0 and 50 m water depth. An evaluation of how a spatially variable water velocity field will impact the proposed method, requires a dedicated modeling exercise including 3D modeling. We think that if these 3D spatial variations in the water-velocity field are smooth, the impact on the proposed method would be limited.

In the simple modeling exercise of the response of a gas chimney, we used the mathematical model known as Wood’s equation to suggest the speed of sound of a

bubbly liquid. Wood's equation relates the speed to its void fraction (i.e., fractional volume of gas in bubble form to volume of water) but is valid only below the resonance frequency of the bubbles. Obviously, the speed of sound in a bubbly liquid is dependent upon the volume fraction of the gas phase, the bubble size distribution, and the frequency of the acoustic excitation (see, e.g., Medwin, 2005). For the speed of sound to depend primarily on the gas volume fraction, the excitation frequency has to be sufficiently low, and well below the resonance frequency. The resonance frequency of an individual bubble is proportional to the square root of the ambient pressure, and inversely proportional to the bubble radius. The resonance frequency of a bubble cloud is essentially identical to that of a single air bubble. The resonance frequency of a spherical bubble cloud is given by Carey and Fitzgerald (1993) and Hwang and Teague (2000), and is proportional to the square root of the ambient pressure, inversely proportional to the square root of the air fraction in the water, and inversely proportional to the bubble cloud radius. Because the size of a bubble cloud is much larger than the size of constituent bubbles, the resonance frequency of a bubble cloud is much lower than the resonance frequency of the constituent bubbles. Therefore, before any field experiment is done, active measurements of acoustic properties of signal scattering and transmission through representative bubble chimneys need to be done to investigate the best mathematical model for inversion. Such measurements we expect will reveal not only those frequencies where the transmitted wavefield through the gas chimney is sigificant but also those frequencies where a back-scattered wavefield is strong and useable for gas detection.

This means that it is very likely that the method proposed here should be extended to include two types of wave-propagation: the transmitted wavefield through the gas chimney as well as the back-scattered wavefield from the gas chimney. The gradual shift

between these two potential analysis methods will vary with frequency, and the transition frequency is probably close to the resonance frequency discussed above.

Another potential method that may further enhance the detectability of leakage is to use diffraction analysis (see for instance Moser et al., 2016). Using advanced diffraction analysis might help reduce the need for ultra high-frequency data. The bubbles in the gas leak chimney will cause absorption effects, that lead to corresponding phase shifts in the measured traveltime. A gas cloud of the size discussed in this paper (1-5 m in diameter) could cause resonance effects, scattering, and damping mechanisms that could affect the detectability. Such effects could be double-edged: They could distort the precise picking of abrubt changes in traveltime, but they could also open a possiblitity to detect the damping and backscattering of the signal. The gas chimney will also cause lens effects, that will influence both amplitudes and traveltimes. This effect has not been investigated in this letter.

CONCLUSIONS

Recent experiments show that the high-frequency (above 1 kHz) signals generated by air gun arrays are sufficiently strong to propagate over distances up to several kilometers in water. We propose to exploit this observation and use the high frequency part of the air gun array signal to detect gas leakage from underlaying sediments into the water column. Simple synthetic ray tracing modeling examples show that these signals can be exploited to detect gas leakage into the water layer. The proposed method takes advantage of any dense receiver array available at the seabed, covering for instance a hydrocarbon field or a CO_2 storage site. A gas chimney with a circular radius of 5 m gives time delays of more than 10 ms, which we think is detectable using conventional air gun arrays and a permanent receiver grid at the seabed.

ACKNOWLEDGMENTS

ML thanks the Norwegian Research Council for financial support to the ROSE consortium at NTNU. We want to thank Deyan Draganov, Jon-Fredrik Hopperstad and two anonymous reviewers for constructive comments and suggestions that improved this letter.

REFERENCES

Aki, K. and P. G. Richards, 2009, Quantitative Seismology, University Science Books, 2nd edition, ISBN 978-1-891389-63-4.

Barkved, O.I., 2004, Continuous seismic monitoring, 74th Annual International Meeting, The Society of Exploration Geophysicists, 2537-2540.

Calvert, R., 2005, Insights and methods for 4D reservoir monitoring and characterization, EAGE/SEG Distinguished Instructure Short Course, **8**.

Carey, W. M and J. W. Fitzgerald, 1993, Low-frequency noise from breaking waves: Natural Physical Sources of Underwater Sound, in B. R. Kerman, Ed., Kluwer Academic, 277–304.

Coste, E., D. Gerez, H. Groenaas, O. P. Larsen, M. Wolfstirn, J. F. Hopperstad, R. Laws*, J. Norton, and M. Padula, 2014, Attenuated high-frequency emission from a new design of air-gun. SEG Technical Program Expanded Abstracts 2014, 132-137.

Etiope, 2015, Natural Gas Seepage - The Earth's Hydrocarbon Degassing, Springer, DOI 10.1007/978-3-319-14601-0_1.

Hovland, M. and A. G. Judd, 1988, Seabed pockmarks and seepages. Impact on geology, biology and the marine environment, Graham and Trotman Ltd. London, 293 pp.

Hwang, P. A. and Teague, W. J., 2000, Low-Frequency Resonant Scattering of Bubble Clouds: Journal of Atmospheric and Oceanic Technology, **17**, 847-853.

Landrø, 1999, Repeatability issues of 3-D VSP data, Geophysics, **64**, 1673-1679.

Landrø, M., O.A. Solheim, E. Hilde, B.O. Ekren and L.K. Strønen, 1999, The Gullfaks 4D study, Petroleum Geoscience, **5**, 213-226.

Landrø, M., 2011, Seismic monitoring of an old underground blowout – 20 years later, First Break, **29**, 39-48.

Landrø, M., L. Amundsen and D. Barker, 2011, High-frequency signals from air-gun arrays, Geophysics, **76**, Q19-Q27.

Landrø, M., Y. Ni and L. Amundsen, 2016, Reducing high-frequency ghost cavitation signals from marine air-gun arrays, Geophysics, **81**, P47-P60.

Medwin, H., 2005, Sounds in the sea. From ocean acoustics to acoustical oceanography: Cambridge University Press.

Moser, T.J., B. Arntsen, S. Johansen, E. B. Raknes and S. Sangesland, 2016, Surface seismic monitoring while drilling using diffractions – concept and field data example, SEG Technical Program Expanded Abstracts 2016, 662-666.

Osdal, B. and M. Landrø, 2011, Estimation of changes in water column velocities and thicknesses from time lapse seismic data, Geophysical Prospecting, **59**, 295-309.

Thomspon, M., M. Andersen, R. M. Elde, S. S. Roy and S. M. Skogland, 2015, The startup of Permanent Reservoir Monitoring for Snorre and Grane, 77th EAGE Conference, Expanded Abstract, Tu N101 01.

Wood, A.W., 1955, A textbook of Sound, The MacMillan Co., New York, 360 pp.

FIGURE CAPTIONS

Figure 1: Bird view sketch showing a circular gas chimney with radius *a* at a distance *d* from the source (marked by a star). The recorded high frequency signal is recorded by a hydrophone (black triangle) at an offset distance *x.* The distance between the source and the receiver line is *y,* and the source receiver distance is *z*. We assume that the P-wave velocity inside the circle is significantly less that the surrounding water. The dashed line shows the situation if the receiver line is rotated by an angle φ. *x'* and *y'* represent the coordinates to the new rotated receiver line. The grey triangle shows the receiver position for the rotated line.

Figure 2: Top: Traveltime curves for the experiment shown in Figure 1: Without a chimney (solid line), chimney with a radius of 5 m (dashed line) and chimney with a radius of 1 m (dotted line). Middle: Traveltime curves for the experiment shown in Figure 1, where the receiver line is rotated by 30 degrees. The zero offset position is defined by the shortest distance from the source to the receiver line. Experiment with a 5 m radius gas leakage chimney is shown by a dashed line, and without by the solid line. Bottom: Intersections for those source-receiver pairs that have intersected the gas anomaly (red circle of radius 1 m) with a relative time delay of more than 0.25 %.To avoid overlapping events uniform random noise have been added to the estimated intersections.

Figure 3: (a) Measured unfiltered signatures of the full array at near offset (solid line) and far offset (225 m; dashed line). (b) Same signatures after 1-5 kHz bandpass filtering, absolute value and smoothing. (c) Normalized versions of the signals shown in b). (d) Normalized version of the signals after 5-10 kHz bandpass filtering.

Figure 4: Crosscorrelation between near- and far-offset traces. Unfiltered version (solid line) shows a negative shift of -1.4 ms. The corresponding time lags for data filtered by a 1-5 kHz (dashed line) and a 5-10 kHz (dotted line) bandpass filter are 2.1 and 2.6 ms.

Figure 5: Signature of a 300 cubic inch air gun filtered with various filters: No filter (black), 2-10 kHz (red), 10-15 kHz (blue), 18-22 kHz (purple), 30-60 kHz (green). The dominant frequency of the echo sounder is 20 kHz, and hence we see the regular peaks (approximately 8 ms interval) on the purple curve.

FIGURES

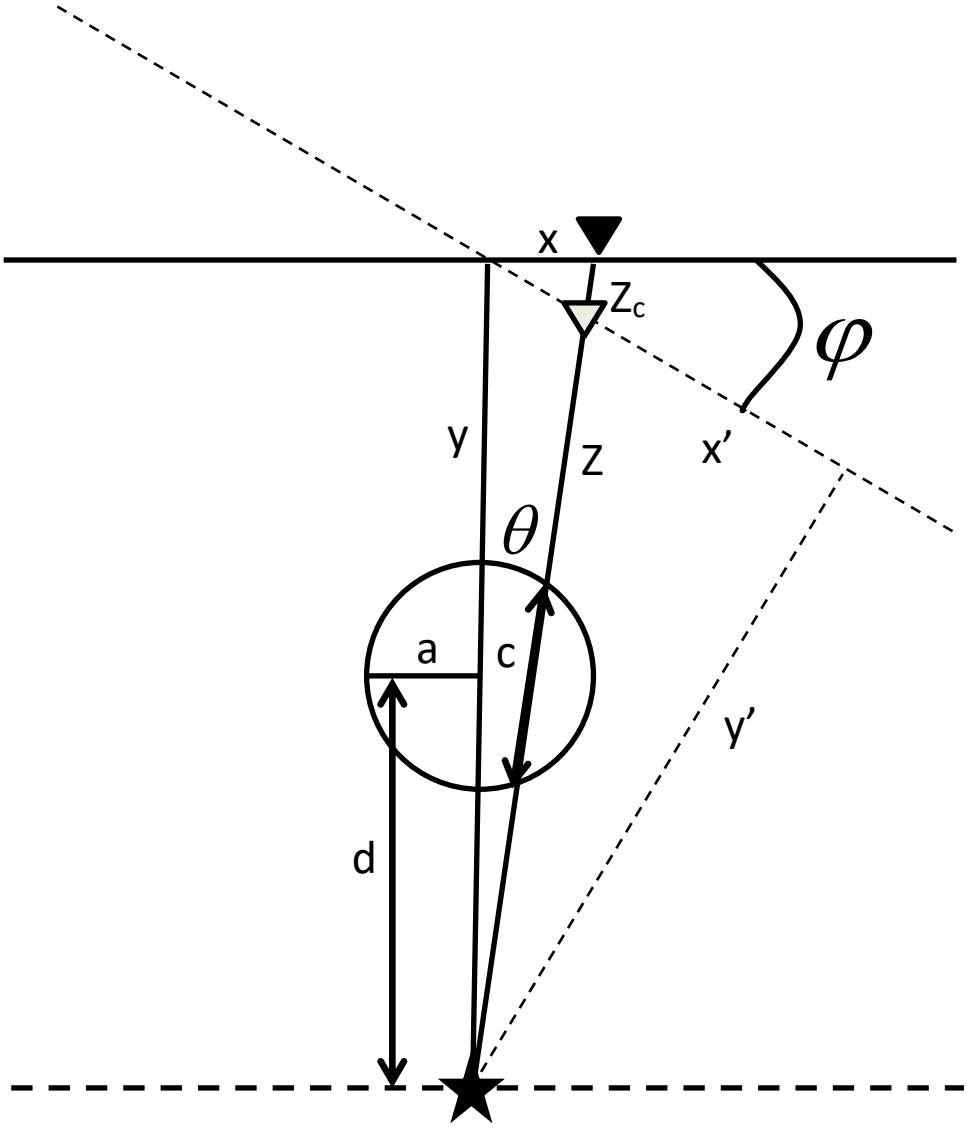

Figure 1: Bird view sketch showing a circular gas chimney with radius *a* at a distance *d* from the source (marked by a star). The recorded high frequency signal is recorded by a hydrophone (black triangle) at an offset distance *x.* The distance between the source and the receiver line is *y,* and the source receiver distance is *z*. We assume that the P-wave velocity inside the circle is significantly less that the surrounding water. The dashed line shows the situation if the receiver line is rotated by an angle φ. *x'* and *y'* represent the coordinates to the new rotated receiver line. The grey triangle shows the receiver position for the rotated line.

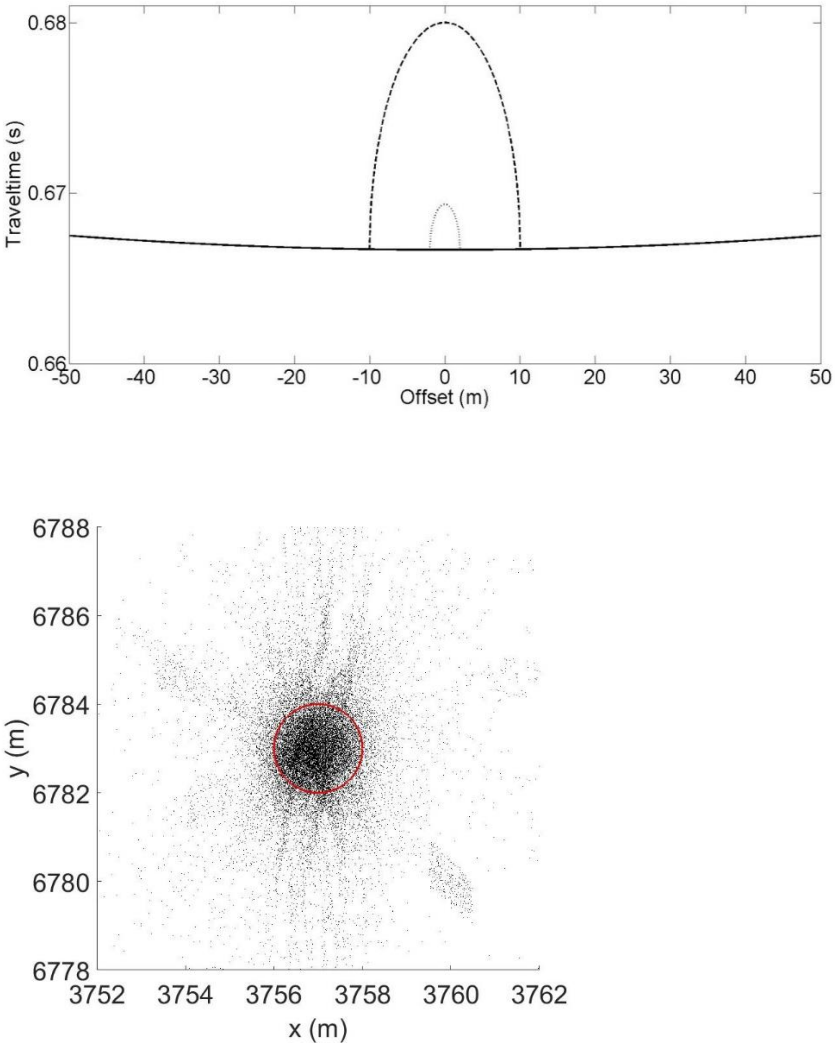

Figure 2: Top: Traveltime curves for the experiment shown in Figure 1: Without a chimney (solid line), chimney with a radius of 5 m (dashed line) and chimney with a radius of 1 m (dotted line). Bottom: Intersections for those source-receiver pairs that have intersected the gas anomaly (red circle of radius 1 m) with a relative time delay of more than 0.25 %.To avoid overlapping events uniform random noise have been added to the estimated intersections.

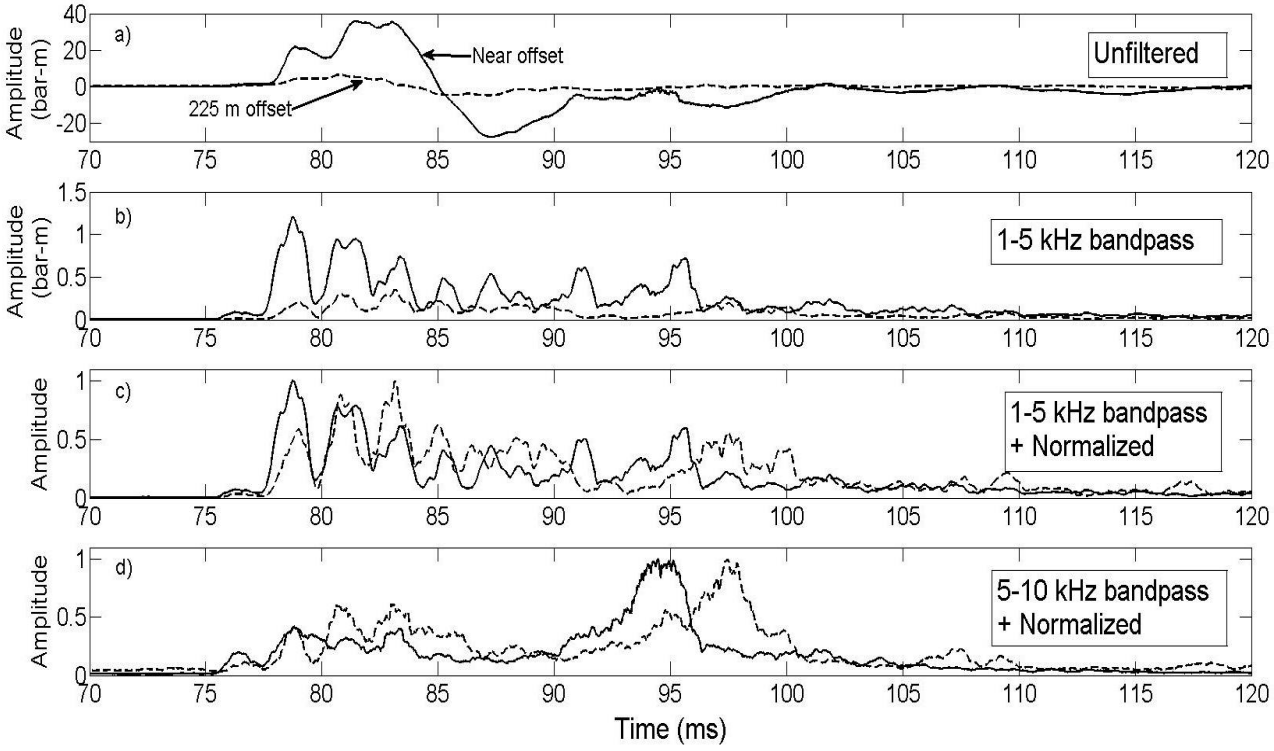

Figure 3: (a) Measured unfiltered signatures of the full array at near offset (solid line) and far offset (225 m; dashed line). (b) Same signatures after 1-5 kHz bandpass filtering, absolute value and smoothing. (c) Normalized versions of the signals shown in b). (d) Normalized version of the signals after 5-10 kHz bandpass filtering.

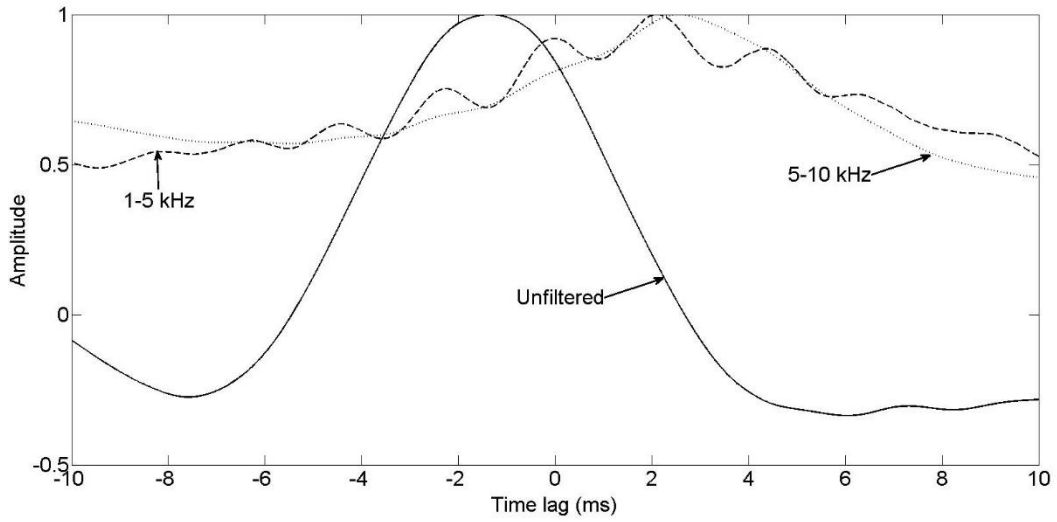

Figure 4: Crosscorrelation between near- and far-offset traces. Unfiltered version (solid line) shows a negative shift of -1.4 ms. The corresponding time lags for data filtered by a 1-5 kHz (dashed line) and a 5-10 kHz (dotted line) bandpass filter are 2.1 and 2.6 ms.

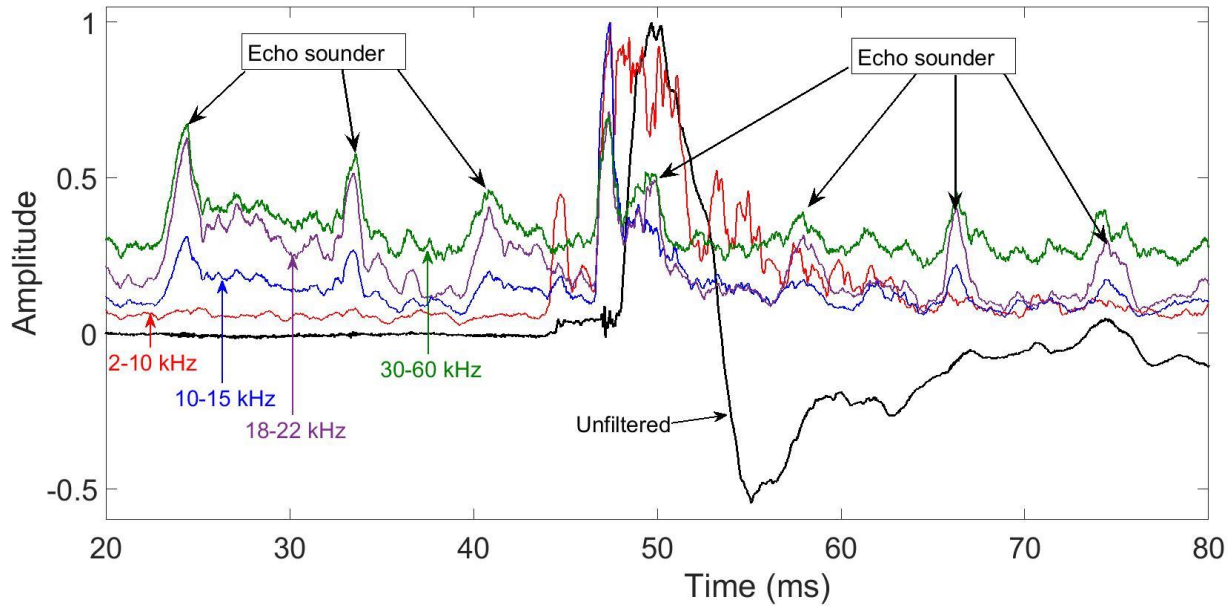

Figure 5: Signature of a 300 cubic inch air gun filtered with various filters: No filter (black), 2-10 kHz (red), 10-15 kHz (blue), 18-22 kHz (purple), 30-60 kHz (green). The dominant frequency of the echo sounder is 20 kHz, and hence we see the regular peaks (approximately 8 ms interval) on the purple curve.